

An Autonomous Real-Time Charging Strategy for Plug-In Electric Vehicles to Regulate Frequency of Distribution System With Fluctuating Wind Generation

Shiwei Xia, *Member, IEEE*, S. Q. Bu[✉], *Senior Member, IEEE*, Xiao Luo, Ka Wing Chan[✉], *Member, IEEE*, and Xi Lu

Abstract—Plug-in electric vehicles (PEVs) could provide valuable ancillary service for power systems with intermittent renewables. This paper proposes a charging model of a large amount of PEVs to mitigate the high-level wind power fluctuations in a distribution network so as to regulate system frequency. With the prerequisite that all PEV daily driving patterns are completely satisfied, the PEV charging power is economically allocated to counterbalance the wind generation intermittency. Afterward, a center-free control scheme based on the consensus algorithm is designed for PEVs to share the fluctuating wind generation in a fully distributed manner. The scheme is robust and flexible to practical PEV charging behaviors including arrival and departure time, initial and desired SOC, as well as the frequently changed departure time. Comprehensive simulations on a distribution system with coal and diesel generators, several wind farms and 2000 PEVs demonstrate that the proposed PEV charging scheme could effectively regulate the system frequency in the real time while the PEV users' charging requirements could be flexibly satisfied.

Index Terms—Daily driving patterns, fully distributed control, frequency regulation, optimal charging model, plug-in electric vehicles.

NOMENCLATURE

$C_{\text{batt},i}$	Battery capacity of PEV _i .
C_{nom}	Coulomb capacity in Ah of PEV battery.

Manuscript received March 21, 2017; revised July 3, 2017; accepted July 20, 2017. Date of publication August 29, 2017; date of current version March 20, 2018. This work was supported in part by the Hong Kong Polytechnic University under Startup Fund Research Project (1-ZE68), in part by the National Key Research and Development Program of China under Grant 2016YFB0900100, in part by the Support Program for the Excellent Talents in Beijing City (2016000020124G079), in part by the Beijing Natural Science Foundation under Grant 3174057, and in part by the Fundamental Research Funds for the Central Universities under Grant 2016MS14. Paper no. TSTE-00262-2017. (*Corresponding author:* S. Q. Bu.)

S. Xia is with the State Key Laboratory of Alternate Electrical Power System with Renewable Energy Sources, North China Electric Power University, Beijing 102206, China, and also with the Hong Kong Polytechnic University, Hong Kong (e-mail: s.w.xia@ncepu.edu.cn).

S. Q. Bu, K. W. Chan, and X. Lu are with the Department of Electrical Engineering, The Hong Kong Polytechnic University, Kowloon, Hong Kong (e-mail: siqi.bu@polyu.edu.hk; eekwchan@polyu.edu.hk; 15901056R@connect.polyu.hk).

X. Luo is with the Department of Investment Planning, Huadian Power International Corporation, Ltd., Beijing 100031, China (e-mail: luo.xiao.peter@connect.polyu.hk).

Color versions of one or more of the figures in this paper are available online at <http://ieeexplore.ieee.org>.

Digital Object Identifier 10.1109/TSTE.2017.2746097

E_i	Required amount of energy to finish the desired SOC of PEV _i .
$P_{\text{act},i,t}$	Actual power output of wind farm i at time t .
$P_{\text{fore},i,t}$	Forecasting power output of wind farm i at timeslot t .
$P_{i,\text{fluc}}(t)$	Fluctuating power output of wind farm i at timeslot t .
$\bar{P}_{i,\text{fluc}}(t)$	Average fluctuating power output estimated by PEV _i at timeslot t .
V_{nom}	Nominal voltage of PEV battery.
V_{oc}	Battery terminal voltage.
V_w	Actual wind speed.
$V_{w\text{a}}$	Average component of wind speed.
$V_{w\text{g}}$	Gust component of wind speed.
$V_{w\text{r}}$	Ramp component of wind speed.
V_{ws}	Filtered wind speed.
V_{wt}	Turbulence component of wind speed.
d_{ij}	Communication coefficient between agent i and agent j .
$\eta_{p,i}$	Charging efficiency of PEV _i .
τ_w	Time constant of wind speed filter.
$\omega_i(t)$	Willingness to pay parameter of PEV _i at timeslot t .
$\bar{\omega}_i(t)$	Average of willingness to pay parameters estimated by PEV _i at timeslot t .
$\omega_{G2v,i}$	Willingness to pay parameter for PEV _i when charging.
$\omega_{v2G,i}$	Willingness to pay parameter for PEV _i when discharging.

I. INTRODUCTION

WITH the increasing concerns on environment and energy conservation, wind power as a typical sustainable and green energy resource has been connected to power systems with a dramatically high penetration level. The remarkable characteristic of wind generation is the natural intermittency, which is difficult to be accurately predicted even for a few hours ahead, and hence it is a pressing need to seek effective solutions for handling these uncertainties and accommodating the highly variable wind generation.

To improve the controllability of a power system with uncertain wind generations, a direct strategy is to reserve a large-scale

spinning capacity of the existing thermal plants to provide sufficient margin for system security [1], [2]. For example, a stochastic security constrained unit commitment model is proposed to determine the minimal spinning reserve to facilitate wind power integration in [3]. These reserve techniques could indeed ensure the system security by requesting a large margin in advance. However, when they take effect in the real time, the highly fluctuating wind power would require frequent on-load cyclic operations of thermal units, which results in detrimental wears and tears to the steam turbine and reduces the longevity of the generation system [4]. In addition, due to the complex dynamics and comparatively large time constants of thermal plants, they might not be capable of catching up with the rapidly changing wind power generation.

On the other hand, nowadays the new advancements in fast-acting devices, such as the battery energy storages, hydroelectric pumped storages, plug-in electric vehicles (PEVs) and diesel generators etc., have enabled them as effective remedies to match the fast wind power fluctuations. In particular, PEVs with nearly zero emissions have been supported at the national level in many countries and surged with a huge quantity, for example 550,000 PEVs serviced in US, 507,000 PEVs in China and 637,000 PEVs in Europe for year 2016 [5]. As grid-connected PEVs can either draw grid-to-vehicle (G2V) power for battery charging or inject vehicle-to-grid (V2G) power for grid energy support, such a large amount of PEVs could be an impressive energy storage in GW level if properly controlled, and PEVs will be very effective in supplying the fast ramping power with proper charging scheme after completing daily driving utilization [6].

In [7], the PEV charging scheme is proposed on the basis of the demand response and game theory to optimize the total charging cost, while in [8], [9] multiple PEVs are coordinated to smooth wind power fluctuations with operational costs reduced. Reference [10] presents a predictive energy management strategy to achieve enhanced fuel economy by using the feedback data of the integrated real-time traffic flow velocity. When adopting PEVs to provide frequency response service, a centralized control scheme is proposed in [11], [12] to assign PEVs optimal charging power for islanded micro-grids. In [13] and [14], the droop control strategy is performed to regulate PEV power outputs according to the frequency deviation of the grid. Besides centralized control, some works have investigated the decentralized charging scheme. In [15] and [16], the aggregated V2G control approach is proposed to suppress the system frequency fluctuation with the help of a control center computing PEV power based on the State of Charge (SOC). The authors of [17] and [18] also design a decentralized PEV charging algorithm to reduce the usage of conventional power plants for power-frequency control. A hierarchical framework to optimize the charging process of PEVs for frequency regulation in a competitive electricity market is proposed in [19] and [20]. The concept of congestion algorithm in Internet traffic control is adopted to propose a novel PEV charging method in smart grid with a good convergence [21]. The congestion algorithm is further improved in [22] with a positive multiplier α to ensure that the congestible resource exactly converges to the actual

wind power to be compensated, and therefore the wind farm fluctuations can be fully neutralized. Since the central information hub is generally needed to gather the necessary information for generating the global signal, all these above are so called the decentralized algorithm. For a large and highly dispersed population of PEVs, however, a fully distributed charging control approach is more desired than a decentralized one.

So far, the state-of-the-art of PEVs for regulating wind power fluctuations is mainly investigated in the viewpoint of the power grid, while the PEV driving patterns and their utilities are not completely addressed yet. Therefore, as the first incentive, this paper proposes a novel PEV charging model to regulate system frequency, maximize PEV total utility and satisfy individual PEV daily drive patterns simultaneously. In addition, to well fit the scattering feature of PEVs across the charging network, a fully distributed control scheme is proposed to economically share wind power fluctuations among multiple PEVs with plug-in and play flexibility for frequency regulation. The main contributions of this paper include: 1) an original PEV charging model simultaneously considering all PEV total utility, PEV daily driving requirements and system frequency regulation is proposed; 2) To solve the model, a fully distributed charging approach based on the consensus algorithm is designed to economically allocate PEV charging power in the real time; 3) The proposed distributed scheme with plug-in and play characteristic is flexible and robust to the frequent change of PEV charging behaviors; 4) Simulation results demonstrate that wind power fluctuation is well mitigated and system frequency is effectively regulated by the proposed charging scheme.

The rest of this paper is organized as follows. The optimal PEV charging model is first proposed in Section II, and then a fully distributed power-allocating algorithm is designed in Section III followed by the discussion about the overall communication network of distributed PEVs in Section IV. Then three case studies are conducted in Sections V and VI respectively to validate the performance and good scalability of the proposed scheme. Conclusions are drawn in the last section.

II. PEV OPTIMAL CHARGING MODEL FOR MAXIMUM UTILITY AND FREQUENCY REGULATION

In this section, the PEV optimal charging model is proposed to mitigate wind power fluctuations and maximize PEV total utility with daily driving patterns considered. In the following, the fluctuating wind power outputs and the dynamic behavior of PEV battery will be firstly presented, and then the PEV charging model will be derived.

A. Fluctuating Wind Power Outputs

A popular composite model is adopted to simulate the actual wind speed V_w [23], which consists of four parts, the average component V_{wa} , the ramp component V_{wr} , the gust component V_{wg} and the turbulence component V_{wt}

$$V_w(t) = V_{wa}(t) + V_{wr}(t) + V_{wg}(t) + V_{wt}(t) \quad (1)$$

The details of V_{wa} , V_{wr} , V_{wg} and V_{wt} can be found in [23]. To smooth the high-frequency wind speed variations over rotor

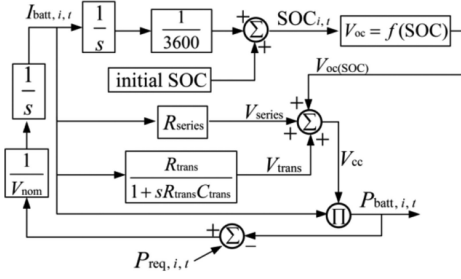


Fig. 1. Model for PEV battery charging dynamics.

surfaces, the filtered wind speed V_{ws} used for determining the mechanical power of wind turbines is the output of a low pass filter as

$$\tau_w \dot{V}_{ws} = -V_{ws} + V_w(t) \quad (2)$$

where τ_w is a time constant relevant to the turbine size. Finally, the actual wind generator output is determined from the speed-power curve of wind turbine as (3) [24].

$$P_{act,i,t} = \begin{cases} 0, & V_{ws} \leq V_{cut-in} \text{ or} \\ & V_{ws} \geq V_{cut-off} \\ 0.5\rho\pi R_{wt}^2 C_p(\beta, \lambda) V_{ws}^3, & V_{cut-in} < V_{ws} \leq V_{rated} \\ P_{rated}, & V_{rated} < V_{ws} < V_{cut-off} \end{cases} \quad (3)$$

where ρ is the air density; R_{wt} is the radius of the rotor; C_p is the performance coefficient; β is the blade pitch angle; λ is the tip-speed ratio; V_{cut-in} , V_{rated} and $V_{cut-off}$ are the cut-in, rated and cut-off wind speed, respectively. For wind farm i , the wind power fluctuation is defined by

$$P_{i,\text{fluc}}(t) = P_{act,i,t} - P_{fore,i,t} \quad (4)$$

$P_{i,\text{fluc}}(t)$ is either positive or negative indicating the necessary charging or discharging power of PEVs.

B. PEV Battery Charging Dynamics and Daily Utilization Requirements

1) *PEV Battery Charging Dynamics:* In this paper, the battery is modeled as a Thevenin-based voltage source in series with an internal resistance R_{series} and a paralleled RC network (consisting of the resistance R_{trans} and capacitor C_{trans}). The battery terminal voltage is related to SOC and defined as a non-linear term of SOC by Nernst equation.

$$V_{oc} = V_{nom} + \alpha(RT/F) \ln(SOC/(C_{nom} - SOC)) \quad (5)$$

where α is a sensitivity parameter of V_{oc} to SOC; R , F and T are the gas constant, the Faraday constant and battery temperature, respectively. When SOC is kept within a range of 10%–95% to preserve battery life, R_{series} , R_{trans} and C_{trans} can be approximated as constants with typical values obtained from [25] shown in Table I.

The dynamics of battery charging could be modeled by the block diagram in Fig. 1, which mainly includes two integral and one inertial elements [25]. In Fig. 1, $P_{req,i,t}$ is the tracking reference of PEV charging/discharging power, which is the op-

timal variable $x_i(t)$ of (19) or $x_{i-local}(t)$ of (23) calculated in Section II-C, and $P_{batt,i,t}$ is the actual power output of PEV.

For PEV $_i$ with the present SOC ($SOC_{i,t}$), the required amount of energy to finish the desired SOC ($SOC_{i,Ti}$) can be calculated by integrating the V_{oc} as follows

$$\begin{aligned} Ei = & \int_{SOC_{i,t}}^{SOC_{i,Ti}} V_{oc} dSOC = V_{nom} (SOC_{i,Ti} - SOC_{i,t}) \\ & + \alpha \frac{RT}{F} C_{nom} \ln \left(\frac{C_{nom} - SOC_{i,Ti}}{C_{nom} - SOC_{i,t}} \right) \\ & + \alpha \frac{RT}{F} SOC_{i,Ti} \ln \left(\frac{SOC_{i,Ti}}{C_{nom} - SOC_{i,Ti}} \right) \\ & - \alpha \frac{RT}{F} SOC_{i,t} \ln \left(\frac{SOC_{i,t}}{C_{nom} - SOC_{i,t}} \right) \end{aligned} \quad (6)$$

2) *Willingness to Pay Parameter for Driving Patterns:* The key parameters relevant to PEV charging behaviors include the arrival time and initial SOC when PEVs are plugged in for charging, and the departure time and destination SOC when PEVs are plugged out for driving. These daily driving patterns should be considered properly for PEVs charging. In the paper, a term named the willingness to pay (WTP) parameter, based on the battery energy capacity (BEC) that can be fulfilled before PEV departure and need to be fulfilled from the current SOC to the destination SOC, is defined to synthesize all factors of driving patterns and indicate the urgent level of PEV charging requests as follows.

When the wind power fluctuation $P_{i,\text{fluc}}(t)$ is positive, the G2V power is needed with PEV being charged accordingly and the WTP parameter of PEV $_i$ at t is defined as

$$\begin{aligned} \omega_{G2V,i}(t) &= 1 / \underbrace{(P_{i,\max} \cdot \eta_{p,i} \cdot (Ti - t) / C_{batt,i})}_{\text{term 1}} - \underbrace{Ei / C_{batt,i}}_{\text{term 2}} \end{aligned} \quad (7)$$

where t and T_i are the present time and planned departure time of PEV $_i$, respectively; Ei is the amount of energy required from the current SOC to the destination SOC of PEV $_i$, which is calculated in (6). The term 1 and term 2 of (7) represent the normalized BEC that can be fulfilled before the planned departure time and to be fulfilled from the current SOC to the destination SOC, respectively. The difference between them is the BEC margin, which indicates how desirous a PEV is to have G2V power.

On the other hand, one PEV which hungers for G2V power should be very undesirous to supply V2G power. In other words, a large value of $\omega_{G2V,i}$ should correspond to a small value of $\omega_{V2G,i}$. Therefore, when the wind power fluctuation $P_{i,\text{fluc}}(t)$ is negative, the V2G power is needed and PEV should be discharged accordingly with the WTP parameter defined as

$$\begin{aligned} \omega_{V2G,i}(t) &= 1 / \omega_{G2V,i} = (P_{i,\max} \cdot \eta_{p,i} \\ &\cdot (Ti - t) - Ei) / C_{batt,i} \end{aligned} \quad (8)$$

When multiple PEVs are utilized to counterbalance the wind power fluctuations, with the charging/discharging process going on, some PEVs will lose the discharging ability while some are

fully charged for the departure, and therefore the status of PEVs can be divided into three categories: the responsive state with grid-connected, nonresponsive state with grid-connected, and grid-disconnected state as follows

$$(P_{i,\max} \cdot \eta_{p,i} \cdot (T_i - t) - E_i)/C_{\text{batt},i} > \text{BEC}_{\text{threshold}} \quad (9.a)$$

$$0 < (P_{i,\max} \cdot \eta_{p,i} \cdot (T_i - t) - E_i)/C_{\text{batt},i} \leq \text{BEC}_{\text{threshold}} \quad (9.b)$$

$$E_i = 0 \quad (9.c)$$

For (9.a), PEV_i is in responsive state only if its BEC margin is greater than a preset threshold $\text{BEC}_{\text{threshold}}$, which means that PEV_i is not urgent to charge power for departure and could participate in charging or discharging properly to neutralize wind power fluctuations. As time t grows and PEV_i approaches its planned departure time T_i , the can-be-fulfilled BEC of PEV_i keeps decreasing at the rate of its maximum charging power P_{\max} , and this leads to the decreasing BEC margin over time. When the margin drops below the preset threshold value, PEV_i will withdraw from the wind power compensation scheme and switch to a nonresponsive state (corresponding to (9.b)). Afterwards, the nonresponsive PEV_i will be charged with the maximum rated power $P_{i,\max}$ for daily driving utilization. Once the desired SOC of PEV_i is completed with $E_i = 0$, it will be disconnected from the power network by the smart socket (corresponding to (9.c)).

C. Maximal Profit Surplus and Frequency Regulation Model for Multiple PEVs

The following proposed PEV charging scheme can be used to provide frequency regulation service in a real-time electricity market. This market is designed and operated by the distribution system operator (DSO), and PEV users are the active participants in the market to bid their frequency regulating capacities. Since conflicts of interests coupled with frequency regulation services exist among multiple PEVs, an effective model capable of simultaneously optimizing the PEV power and participating in frequency regulation is highly needed in a competitive electricity market. As the technical content of the proposed scheme is the focus in this paper, the detailed market framework for the application of the proposed scheme will be fully investigated in the future.

In this market, the designed PEV charging scheme should benefit both PEV owners and power industry utility. It is obvious that the utility can benefit from the effective frequency regulation such as replacing part of the expensive coal-fired fast reserve with grid-connected PEVs and reducing some extra conventional spinning reserves. On the other hand, economic incentives should be offered to PEV owners for their frequency regulation services due to the battery degradation and losses cost incurred from the charging/discharging process. As investigated in [22], [26], [27], when PEV battery is subjected to frequent charging/discharging events, the battery degradation and loss are closely related to the amount of energy processed by the battery and the rate cycling of the power. The battery degradation and loss cost can be evaluated based on

the amount of energy processed by the PEV battery during its charging/discharging process and the variations of battery power between any two consecutive intervals. In another aspect, the PEV owners would obtain revenues from providing the reserve capacity of frequency regulation during both charging and discharging process for wind power compensation. In the authors' previous work [22], an economic analysis was conducted for the battery degradation and loss cost against the revenue of frequency regulation, and the analysis demonstrated that the PEV owner could overall gain a net cost saving based on the state-of-art average hourly regulation market clearing price in PJM. Moreover, since the grid-connected PEVs are able to create economic benefit for both PEV owners and power utility, the utility could even further relinquish a share of the profits by providing a better incentive scheme of frequency regulation services for PEV owners thus to make the charging scheme more attractive to PEV owners and encourage them to participate more in the market.

Based on the above discussion, we made four general assumptions to form the PEV charging scheme in following section. 1) Firstly, there is a proportionally fair pricing based energy market designed and operated by the DSO, in which the PEV owners who are willing to pay the higher prices would have a larger share of the energy capacity [21]. 2) Secondly, encouraged by an attractive financial compensation to PEV owners, PEV users are willing to leave their PEVs during a certain period for charging/discharging (say, starting around 22:00 after they arrive home until the departure time 8:00 of next morning) as long as the vehicles can achieve satisfactory SOC before the departure. 3) Thirdly, the static security constraints such as feeder thermal capacity limits and nodal voltages limits are not considered in the proposed PEV charging scheme, as the focus of this paper is to regulate system frequency. 4) Finally, the PEV charging facilities are properly configured with smart sockets that could interact with a large number of PEVs and control the PEV charging process based on proper communication networks.

With these assumptions, inspired by [21] and [28], a discrete time system where n PEVs share some power demands (such as the wind generation fluctuations in this paper) is considered. In each time slot t , PEV_i has a quantity of $x_i(t)$ charging/discharging demands, and the unit Market Price (MP) of demands is determined as a function of the aggregated demands $\sum x_i(t)$ arriving in that time slot as

$$p(t) = a \left[\sum_{i=1}^n x_i(t)/C(t) \right]^k \quad (10)$$

where $p(t)$ is the MP at time t ; n is the number of PEV users; $x_i(t)$ is the power of PEV_i at time t ; $C(t)$ is the network capacity available at time t ; a and k are constants. Each PEV is evaluated by a non-decreasing utility function, and a typical utility function is logarithmic [21], [28]

$$u_i(t) = \omega_i(t) \log x_i(t) \quad (11)$$

where $\omega_i(t)$ is the WTP parameter calculated by (7) or (8). The individual profit surplus is equal to the utility minus the cost

$$V_{i\text{-profit}} = u_i(t) - x_i(t)p(t) = \omega_i(t) \log x_i(t) - x_i(t)p(t) \quad (12)$$

For multiple PEVs, the objective of the proposed charging model is to maximize the total profit surplus

$$\max \sum_{i=1}^n V_{i\text{-profit}} = \max \sum_{i=1}^n [\omega_i(t) \log x_i(t) - x_i(t)p(t)] \quad (13)$$

To keep the power balance for system frequency regulation, all PEVs total power outputs should exactly match the total fluctuating wind generation as

$$\sum_{i=1}^n x_i(t) = \sum_{i=1}^m P_{i\text{-fluc}}(t) \quad (14)$$

The proposed PEV charging model includes (7) or (8), (10), (13) and (14). To solve the model, the Lagrangian multiplier method is used to transform the proposed model into a non-constrained optimal problem as

$$\max \sum_{i=1}^n V_{i\text{-profit}} = \max \left\{ \begin{array}{l} \sum_{i=1}^n [\omega_i(t) \log x_i(t) - x_i(t)p(t)] \\ + \lambda \left[\sum_{i=1}^m P_{i\text{-fluc}}(t) - \sum_{i=1}^n x_i(t) \right] \end{array} \right\} \quad (15)$$

Substitute (14) into (15), we could rewrite (15) as

$$\max \left\{ \begin{array}{l} \sum_{i=1}^n [\omega_i(t) \log x_i(t)] - p(t) \sum_{i=1}^m P_{i\text{-fluc}}(t) \\ + \lambda \left[\sum_{i=1}^m P_{i\text{-fluc}}(t) - \sum_{i=1}^n x_i(t) \right] \end{array} \right\} \quad (16)$$

The second term in (16) is constant after $p(t)$ is determined, and therefore maximizing (16) is equivalent to optimizing the following problem

$$\max \sum_{i=1}^n V_{i\text{-profit}} = \max \left\{ \begin{array}{l} \sum_{i=1}^n [\omega_i(t) \log x_i(t)] \\ + \lambda \left[\sum_{i=1}^m P_{i\text{-fluc}}(t) - \sum_{i=1}^n x_i(t) \right] \end{array} \right\} \quad (17)$$

and the optimal solution of PEV_i charging power is

$$\lambda = \sum_{i=1}^n \omega_i(t) / \sum_{i=1}^m P_{i\text{-fluc}}(t) \quad (18)$$

$$x_i(t) = \omega_i(t) / \lambda = \omega_i(t) / \sum_{i=1}^n \omega_i(t) \times \sum_{i=1}^m P_{i\text{-fluc}}(t) \quad (19)$$

While for the individual PEV, to obtain its own maximal profit surplus, the optimal MP should be settled by optimizing (12) and PEV_i optimal charging power is

$$x_{i\text{-local}}(t) = \omega_i(t) / p(t) \quad (20)$$

Considering the power balance constraint (14) for frequency regulation and summing over index i on both sides of (20), MP

can be calculated as

$$p(t) = \sum_{i=1}^n \omega_i(t) / \sum_{i=1}^n x_{i\text{-local}}(t) = \sum_{i=1}^n \omega_i(t) / \sum_{i=1}^m P_{i\text{-fluc}}(t) \quad (21)$$

accordingly, the parameter $C(t)$ in (10) is

$$C(t) = a \times \left[\sum_{i=1}^m P_{i\text{-fluc}}(t) \right]^{(k+1)/k} / \left[\sum_{i=1}^n \omega_i(t) \right]^{1/k} \quad (22)$$

and the local optimal solution (20) for the individual PEV is

$$x_{i\text{-local}}(t) = \omega_i(t) / p(t) = \omega_i(t) / \sum_{i=1}^n \omega_i(t) \times \sum_{i=1}^m P_{i\text{-fluc}}(t) \quad (23)$$

By comparing (23) with (19), it is clear that for the proposed charging model, when the overall PEVs maximize their total profit surplus, each individual PEV also get the maximal profit surplus from charging network at the same time, and the market price $p(t)$ is exactly the same as the Lagrangian multiplier λ .

With the proposed PEV charging model, all PEVs are coordinated to economically share the wind power fluctuations with solutions indicated by (19) or (23), in which PEV_i could charge or discharge with the ratio of its own WTP over the summation of all WTPs.

III. FULLY DISTRIBUTED CHARGING SCHEME OF PEVS

In Section II, the optimal PEV charging model with daily driving requirement and frequency regulation constraints is presented to maximize total profit surplus, and the optimal solution is derived in (19) or (23), which can be easily calculated in a decentralized manner if there is an information hub to collect all WTPs and wind power fluctuations. However, to nicely fit the wide scattering feature of PEVs in the distribution network and enhance the reliability of PEVs charging control, a fully distributed optimal algorithm based on the consensus theory is proposed in this section.

Consensus algorithm only requires local information of neighboring agents and coordinates to find the global optimal solution. In consensus algorithm, the value affiliated to agent i is updated as [29]–[32]

$$y_i[k+1] = \sum_{j=1}^n d_{ij} y_j[k] \quad (24)$$

where $y_j[k]$ is the local value assigned to agent j at iteration k , $y_j[k+1]$ is the updated value of y_j at iteration $k+1$, and n is the total number of agents participating in the information discovery process, which could be derived from Laplacian matrix of the communication graph [29], [30]. As the *mean metropolis* indicator is distributed and adaptive to changes of communication network topology with converged optimal solution, it is directly introduced to calculate d_{ij} as

$$d_{ij} = \begin{cases} 1/(n_i + n_j + 2) & (j \in N_i) \\ 1 - \sum_{j \in N_i} 1/n_i + n_j + 2 & (i = j) \\ 0 & \text{otherwise} \end{cases} \quad (25)$$

where N_i is the index of neighbor agents connected with agent i , n_i and n_j are the numbers of agents connected to agents i and j , respectively. According to the consensus theory [29], [30], when $k \rightarrow \infty$ all state variables will be stable

$$\lim_{k \rightarrow \infty} y_i[k] = \frac{1}{n} \sum_{j=1}^n y_j[0] = \bar{y} \quad (26)$$

Equation (26) indicates all the state variables will converge to the average value \bar{y} of the initial value $y_j[0]$.

To solve the proposed model in Section II in a fully distributed manner, the crux is to calculate the Lagrangian multiplier in (18) locally. According to (26), the numerator and denominator of (18) could be iteratively estimated to be

$$\sum_{i=1}^n \omega_i(t) = n \times \overline{\omega_i(t)} = n \times \lim_{k \rightarrow \infty} \omega_i(t)[k] \quad (27)$$

$$\sum_{i=1}^m P_{i,\text{fluc}}(t) = m \times \overline{P_{i,\text{fluc}}(t)} = m \times \lim_{k \rightarrow \infty} P_{i,\text{fluc}}(t)[k] \quad (28)$$

with iteratively updating $\omega_j(t)$ and $P_{j,\text{fluc}}$

$$\omega_i(t)[k+1] = \sum_{j=1}^n d_{ij} \omega_j(t)[k] \quad (29)$$

$$P_{i,\text{fluc}}(t)[k+1] = \sum_{j=1}^m d_{ij} P_{j,\text{fluc}}(t)[k] \quad (30)$$

For (29) and (30), $\omega_i(t)$ and $P_{i,\text{fluc}}(t)$ of PEV $_i$ are updated based on $\omega_j(t)$ and $P_{j,\text{fluc}}$ of its neighboring PEV $_j$. With the increasing of iteration k , $\omega_i(t)[k]$ and $P_{i,\text{fluc}}(t)[k]$ converge to the average value; Then $\sum \omega_i(t)$ and $\sum P_{i,\text{fluc}}(t)$ are calculated by (27) and (28) only using the local value $\omega_i(t)[k]$ and $P_{i,\text{fluc}}(t)[k]$, and consequently the Lagrangian multiplier of PEV $_i$ is calculated by (18) and the optimal power output of PEV $_i$ is determined by (19). Since consensus algorithm could converge well in a few iterations [29]–[32], the maximum iteration k_{\max} is fixed at 100 for the case studies in Sections V and VI. The flowchart of proposed distributed algorithm is presented in Fig. 2.

IV. COMMUNICATION NETWORK IMPLEMENTATION CONSIDERATIONS

There are various candidate technologies both wired (e.g., power line communications and TCP/IP Ethernet) and wireless (e.g., Wi-Fi, cellular, WLAN, TV white spaces and ZigBee) available for two-way communication links of multiple PEVs [21], [33]. Each PEV has an intelligent agent that could control its charging strategy and exchange information (e.g., unbalanced power and the WTP parameters in this paper) with neighboring PEVs via these communication technologies. Among all these communication technologies, ZigBee is the most promising platform for constructing the PEV communication network with the following advantages [33]:

- 1) low power consumption; 2) flexibility to various network topologies; 3) simplicity for device implementing; 4) capability of self-organizing mesh network. In addition, ZigBee's data rate

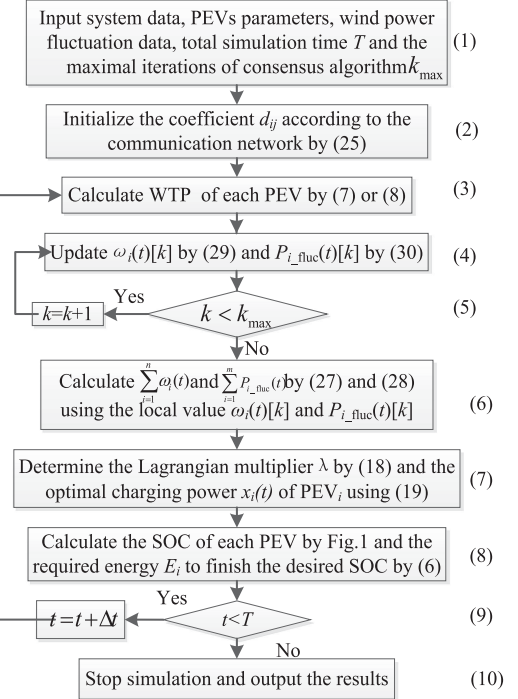


Fig. 2. Flowchart of the proposed PEV charging scheme.

at 2.4 GHz can reach around 250 kb/s to satisfy the estimated bandwidth requirements for PEV applications between 9.6 and 56 kb/s. In particular, its Low cost (e.g., device cost, installation cost and maintenance cost) can boost the commercial deployment of the desired communication networks in a large-scale. As ZigBee based on the IEEE 802.15.4 physical layer of the open system interconnection model and the link layer device enables the network to handle any number of devices, ZigBee could accommodate a large number of communication nodes per network and is very suitable for the connection of numerous distributed PEVs, as investigated and tested in [34] and [35].

ZigBee network has two typical devices, i.e., the Full Function Device (FFD) and ZigBee Coordinator (ZC). ZC is responsible for managing the local ZigBee network, as a root node enabling ZigBee nodes to leave or join the network and also serving as a bridge to other regional networks, and FFD behaves as the end devices (connecting the PEV) which can communicate with the ZC and other FFDs as well as act as an intermediate router node in the ZigBee network. Based on functionalities of the FFDs and ZC, a very flexible communication network can be properly configured as Fig. 3 for conducting the center-free control algorithm proposed in this paper.

This is a hybrid two-layer communication network consisting of the remote networks and local area ZigBee networks. For the inner local area, there are numerous FFDs and ZC attached to PEV chargers to properly form the ZigBee network based on the IEEE802.15.4, by which the individual PEV can freely exchange information such as the unbalanced power demand and WTP parameters with other PEVs. The connectivity of the ZigBee network will determine the reliability of the system, and here a $n-1$ rule could be utilized to design the topology of

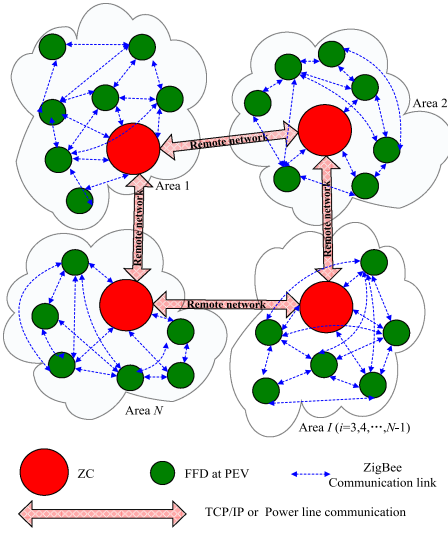


Fig. 3. Overall communication network structure of numerous distributed PEVs.

the communication network, which means that there is no isolated node even if any communication link is disabled. For local ZigBee network, there could be hundreds or even thousands of communication nodes for a ZigBee network and it is very suitable for installing in public charging facilities or community charging piles. To further accommodate tremendous PEVs scattering in a distribution system with long distances, the local ZigBee networks could be easily expanded with the remote network based on the TCP/IP Ethernet or power line communications, in which the multiple regional ZigBee networks are also with highly reliable connections based on certain strategies such as the $n-1$ rules. It can be noted that Fig. 3 is just an overall communication topology, and the detailed implementation of the structure is reserved for future work to align with communication technology standardization for PEV charging in practice.

V. SIMULATIONS

A single-area distribution system shown in Fig. 4 is used to test the proposed PEV charging scheme. The system includes the coal and diesel generators, five wind farms (denoted as WP₁ to WP₅) and 2000 PEVs. As a simplified example for demonstration purposes, these 2000 PEVs are divided into 16 groups evenly (denoted as PEV₁ to PEV₁₆), and the PEVs in the same group connect to one PEV aggregator/station, which have the same initial SOC, arrival time, desired SOC, and planned departure time. In particular, for PEV₄ to PEV₈, there are five wind farms WP₁ to WP₅ nearby and each wind farm connects to the communicating node of the nearby PEV station. In Fig. 4, all PEVs coordinate to counteract the wind power fluctuations, meanwhile the coal and diesel generators act to further keep the whole system power balance with primary frequency control. The system parameters are given in Table I.

A center-free communicating network is implemented in Fig. 4. Each PEV aggregator/station is equipped with an agent (marked as a blue circle in Fig. 4), which is capable of commu-

TABLE I
PARAMETERS OF PEV BATTERY AND DISTRIBUTION SYSTEM

For battery	Value	For AGC	Value
V_{nom}	364.8 V	M	10s
C_{nom}	66.2 Ah	D	12.5 MW/Hz
C_{batt}	24.15 kWh	T_{CG}	0.2 s
α	15	T_{CH}	0.3 s
RT/F	0.02612	I/R_{CG}	20 MW/Hz
R_{series}	0.074 Ω	k_I	0.2 MW/(Hz·s)
R_{trans}	0.047 Ω	T_{DG}	0.1s
C_{trans}	703.6 F	T_d	0.1s
η_p	0.985	I/R_{DG}	8 MW/Hz

nicating with its neighboring agents, and could also 1) calculate the PEV power according (19); 2) update the PEV power-track reference $P_{\text{req},i,t}$ in Fig. 1. It should be noted that the communicating network can be designed to be different from Fig. 4, and the proposed distributed charging scheme can be applied to various network topologies, as long as all PEVs and wind farms are connected by the communicating network. Different network topologies only affect the information-exchanging rate or information sharing efficiency among agents and thus have certain influences on the convergence of the consensus algorithm.

In the following case studies, the typical period from 10 p.m. of the first day to 8 a.m. of the next morning is investigated for the proposed scheme. The battery parameters of PEVs are obtained from commercial Nissan Leaf as shown in Table I with a 220 V/23 A outlet [25], and the maximum allowable charging power is 5.06 kW. The BEC margin threshold is 4%. The agents in the communication network exchange information every 20 milliseconds, while the PEV power reference in Fig. 1 is updated every 2 seconds with WTP parameters recalculated every 30 seconds.

A. Case Study 1 (Demonstration of the Convergence Procedure of the Proposed Charging Scheme)

To demonstrate the convergence of the proposed scheme, PEVs driving patterns are simplified and shown in Table II: the initial SOC of PEV₁ to PEV₁₆ is random in the range [25%, 55%], while the desired SOC are 95% for PEV₁ to PEV₄, 90% for PEV₅ to PEV₈, 85% for PEV₉ to PEV₁₂ and 80% for PEV₁₃ to PEV₁₆. The planned departure time for PEV₁ to PEV₈ is 7 hours after its arrival, and 8 hours for PEV₉ to PEV₁₆. The total fluctuating wind generation is assumed as $P_{\text{flu}} = P_{\text{act}} - P_{\text{fore}}$ in Table III, while the total wind generation fluctuation P_{flu} is allocated to the wind power WP₁ to WP₅ with the ratios of 0.1, 0.15, 0.15, 0.25 and 0.35 respectively, and wind farm power fluctuations are sampled every 8s.

The key capability of the proposed scheme for locally estimating $\sum \omega_i(t)$ and $\sum P_{i,\text{fluc}}(t)$ is firstly investigated for the beginning 2s of 22:00–23:00. Based on the data in Table III, since WP₁ to WP₅ only connects to PEV₄ to PEV₈ respectively, in theory the total wind generation fluctuation estimated locally by each PEV without other information should be $150 \text{ kW} * 16 = 2400 \text{ kW}$ for PEV₄, $225 \text{ kW} * 16 =$

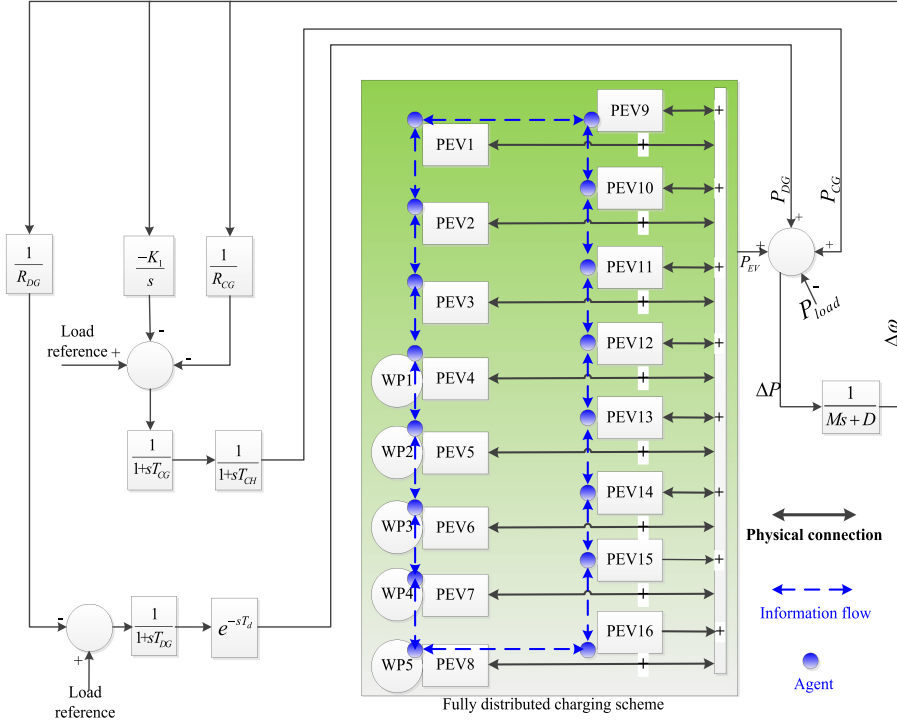


Fig. 4. Configuration of the distribution system with 16 PEVs and 5 wind generators.

TABLE II
ASSUMED PEV USERS' DAILY UTILIZATION REQUIREMENTS

users' needs	SOC_{ini}	SOC_{end}	$T_i(s)$	users' needs	SOC_{ini}	SOC_{end}	$T_i(s)$	
PEV1	0.5042	0.95	25200	PEV9	0.3584	0.85	28800	
PEV2	0.4600			PEV10	0.5066			
PEV3	0.2562			PEV11	0.2536			
PEV4	0.3018			PEV12	0.2673			
PEV5	0.2681			PEV13	0.3496	0.8		
PEV6	0.5061			PEV14	0.2629			
PEV7	0.2668			PEV15	0.5100			
PEV8	0.4067			PEV16	0.3562			

TABLE III
WIND POWER FLUCTUATIONS DURING 22:00–08:00

Time	22:00-23:00	23:00-24:00	00:00-01:00	01:00-02:00	02:00-08:00
Actual wind power P_{act} (kW)	7500	6750	5625	4500	5250
Forecasting Wind power P_{act} (kW)			6000		
Total wind power fluctuation P_{fluc} (kW)	1500	750	-375	-1500	-750
WP1 (kW)	150	75	-37.5	-150	-7.5
WP2 (kW)	225	112.5	-56.25	-225	-112.5
WP3 (kW)	225	112.5	-56.25	-225	-112.5
WP4 (kW)	375	187.5	-93.75	-375	-187.5
WP5 (kW)	525	262.5	-131.25	-525	-262.5

3600 kW for both PEV₅ and PEV₆, 375 kW * 16 = 6000 kW for PEV₇ and 525 kW * 16 = 8400 kW for PEV₈, while other PEVs should estimate a value of zero total wind power fluctuation. Fig. 5 plots the estimated $\sum P_{i,\text{fluc}}(t)$ within the first 200 iterations for validation purpose, and the convergence curves

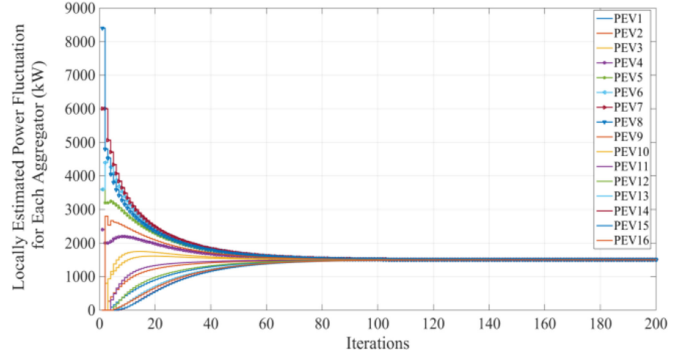


Fig. 5. Convergence of locally estimated wind power fluctuations.

exactly start from 2400 kW, 3600 kW, 3600 kW, 6000 kW and 8400 kW for PEV₄ to PEV₈ respectively, while zero for other PEVs. With the increase of iterations, all PEVs converge to a common value and finally reach at 1500 kW as the approximated total wind generation fluctuations $\sum P_{i,\text{fluc}}(t)$ with 100 iterations. For 100–200 iterations, all agents detect no changes for WP₁ to WP₅.

Similarly, the summation of WTP parameter $\sum \omega_i(t)$ is also locally estimated and the convergence process is shown in Fig. 6. Different from Fig. 5, all curves in Fig. 6 start at non-zero value, and settle down to the converged value. Based on the converged value of $\sum P_{i,\text{fluc}}(t)$ and $\sum \omega_i(t)$ in Figs. 5 and 6, the Lagrangian multiplier λ in (18) could be locally calculated and the optimal PEV power is determined by (19).

From the above analysis, it is clear that the estimation of $\sum P_{i,\text{fluc}}(t)$ and $\sum \omega_i(t)$ relies on the self-evident value

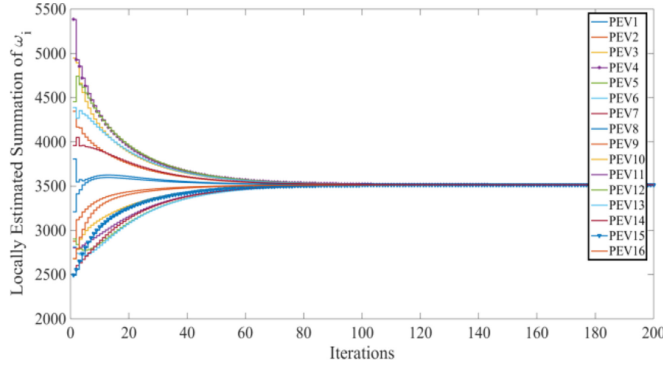


Fig. 6. Convergence of locally estimated WTP $\sum w_i(t)$.

$P_{i,\text{fluc}}(t)$ and $\omega_i(t)$ of agent i , which only exchanges limited information with its neighbours by (29) and (30) instead of collecting information from an all-round hub. On this basis, the Lagrangian multiplier λ and the optimal generation of PEVs are calculated locally, and therefore the proposed approach is a fully distributed PEV charging scheme.

For the remaining time period, the proposed distributed algorithm continues to estimate the total wind power fluctuations $\sum P_{i,\text{fluc}}(t)$ and summation of WTPs $\sum \omega_i(t)$, and a responsive PEV will react to the estimated Lagrangian multiplier and adjust its G2V/V2G power by (19). The total power generation of all responsive PEVs is expected to counteract the wind power fluctuations, and Fig. 7 shows the PEV charging/discharging behaviors during the 10 hours. According to the data in Table III, the positive wind generation fluctuation (1500 kW) during 22:00–23:00 indicates that all PEVs should be charged properly to counteract the wind power surplus, and all PEVs indeed coordinate to charge power correctly in Fig. 7(a). PEV₃ has the smallest initial SOC_{ini} (0.2562), the largest desired SOC_{end} (0.95) and the earlier departure time T_i (25200s), which has resulted in the largest WTP parameter $\omega_i(t)$. Therefore, PEV₃ has the largest charging power during 22:00–23:00. While for PEV₁₅ with SOC_{ini} = 0.51, SOC_{end} = 0.8 and T_i = 28800 s, it is not so urgent compared with other PEVs, and hence it has the smallest charging power. For the period 23:00–24:00, the wind generation fluctuation is also positive but with a smaller value 750 kW, and thus all PEVs are responsive with the smaller charging power compared with that during 22:00–23:00, in which PEV₃ and PEV₁₅ are still charged with the largest and smallest power. For the period 00:00–01:00, the wind fluctuation is reduced to a negative value -375 kW, which indicates that the actual wind generation is smaller than the forecasting wind generation, and all PEVs start to discharge power accordingly. In this period, PEV₃ is with the smallest discharging power while PEV₁₅ is with the largest discharging power. For the next period 01:00–02:00, most PEVs continue to discharge power to compensate the negative wind power fluctuation except PEV₃, which meets the non-responsive criterion at nearly 01:40 (13381s after its arrival), and steps up to the rated power for charging. For the period 02:00–04:00, all PEVs meet the non-responsive criterion one after another and start to charge power only. During period 04:00–06:00, PEV₁ to PEV₈ is with the satisfied SOC_{end} and

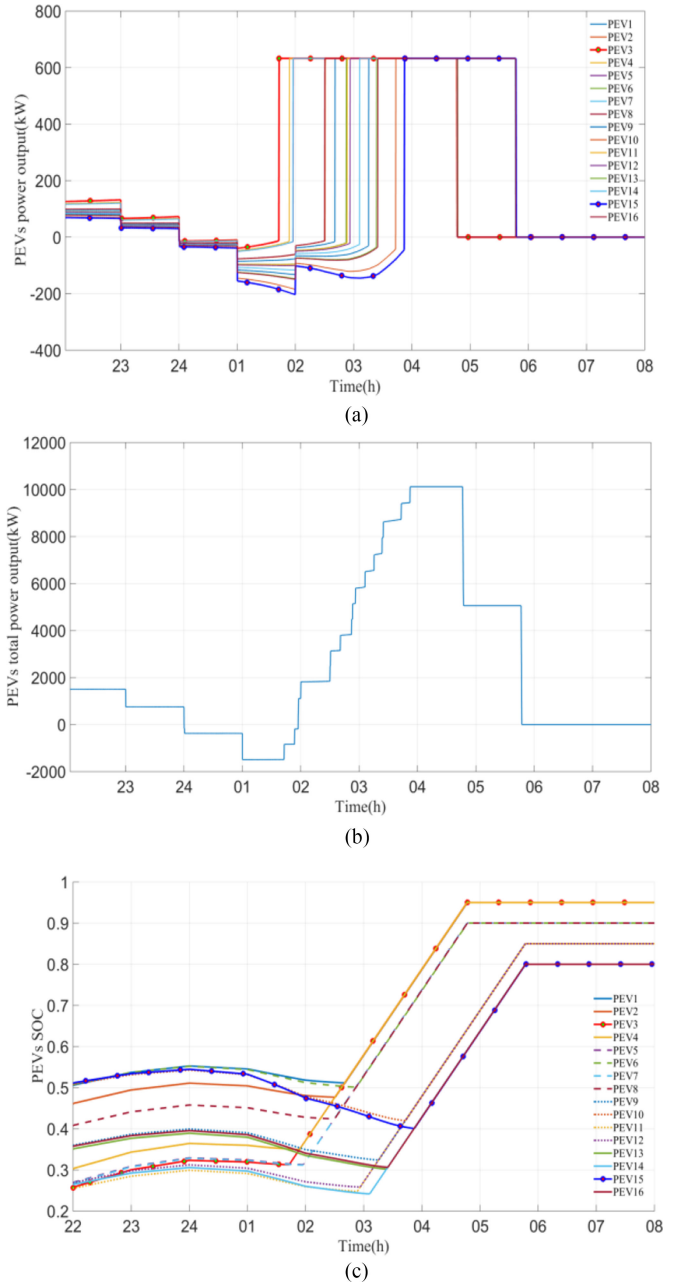


Fig. 7. Charging/discharging power and SOC curves of 16 PEVs. (a) Power output of 16 PEVs. (b) Total power outputs of 16 PEVs. (c) SOC curves of 16 PEVs.

leaves the charging network, and then the SOC_{end} of PEV₉ to PEV₁₆ is satisfied. All PEVs finish the charging tasks for daily driving within the planned departure time T_i .

The total power outputs of PEVs are plotted in Fig. 7(b). It can be seen that for the first three hours 22:00–01:00, all PEVs are responsive to counteract the wind power fluctuation; with time going, more PEVs start to charge power, and the total power output of PEVs gradually steps up to $5.06 * 2000 = 10120$ kW. All PEVs finish the battery-charging task before the departure time and finally the total power output steps down to zero.

The SOC curves are further plotted in Fig. 7(c) along with Fig. 7(a) and (b). It is demonstrated that for 22:00–24:00, all

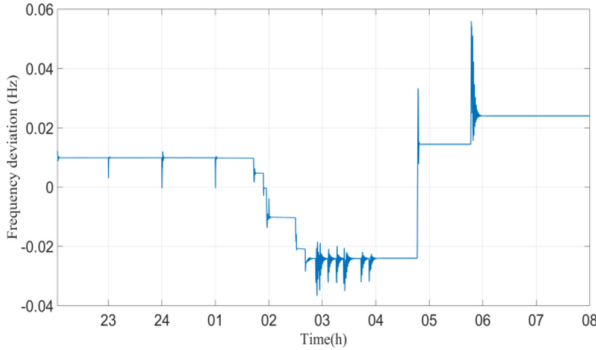


Fig. 8. Frequency deviation of the distribution system.

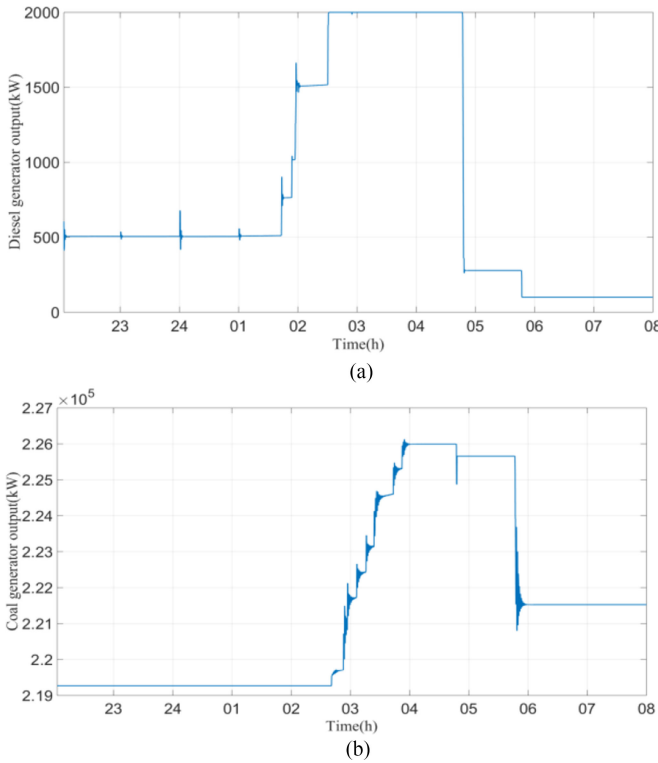


Fig. 9. Power output of the coal and diesel generators. (a) Coal generator power output. (b) Diesel generator power output.

PEVs are with charging power and the SOC is increased; for the period 24:00–01:00, all PEVs start to discharge power with the SOC decreased; for the period 02:00–04:00, as some PEVs are charged with the rated power, the corresponding SOC is increased with a fixed slope. Since PEV₁ to PEV₁₆ has the same maximal rated power, the SOC of all PEVs is increased at the same slope for 02:00–04:00. For 04:00–08:00, PEV₁ to PEV₈ firstly arrive at the desired SOC_{end} and PEV₉ to PEV₁₆ arrive later. Fig. 7(c) also clearly reveals that PEV₃ is the most urgent one to start charging with rated power, while PEV₁₅ is not so urgent and is the last one to be charged with rated power.

Fig. 8 simulates the system frequency deviation during period 22:00–08:00 with the power outputs of coal and diesel generators plotted in Fig. 9. It can be observed that with the proposed charging scheme, the aggregated power outputs of PEVs could exactly counterbalance the wind power generation fluctuation

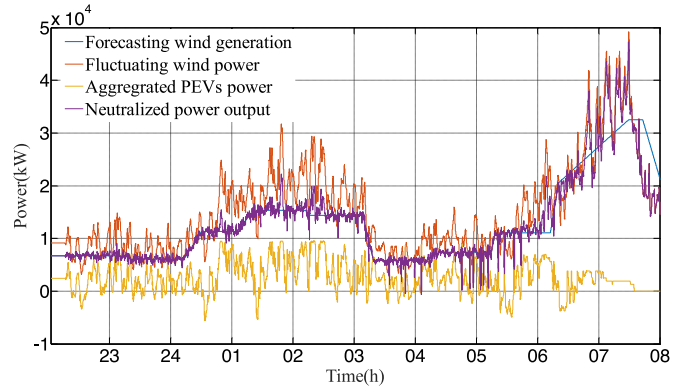


Fig. 10. Neutralized power output with 16 PEVs.

during 22:00–01:00. For 01:00–08:00, as an increasing number of responsive PEVs becomes nonresponsive or even plugged-out, the power compensation provided by PEVs becomes insufficient after 01:40 a.m. and hence the coal and diesel generator need to respond to ensure the power balance with bouncing power output. Since most PEVs step up to the rated charging power during 02:00–04:00, the frequency slightly fluctuates with some burrs during that period as shown in Fig. 8.

B. Case Study 2 (Validation of Frequency Regulation with Various Driving Patterns)

In case study 2, a more practical utilization of PEVs in frequency regulation is demonstrated with the complex parameters setup as: 1) the SOC_{ini} of PEV₁ to PEV₁₆ is randomly generated in the range of [25%, 55%], and the SOC_{end} is 0.9 or 0.95; 2) the departure time T_i of all PEVs is random in 04:00–08:00; 3) the fluctuating wind power is generated based on Section II.A with data from [22], and the forecasting wind generation is assumed to be dynamic with time as shown in Fig. 10, and wind farm power fluctuations are sampled every 8s; 4) to test the plug-in and play capability of the proposed charging scheme, PEV₂ is randomly plugged in for charging power instead of at 22:00, and PEV₁ is accidentally plugged out for emergency usage before 08:00.

The proposed charging scheme tries to coordinate all responsive PEVs to neutralize the fluctuating wind generation in the real time. As shown in Fig. 10, during 22:00–04:00, the total power of all PEVs could perfectly counteract the wind generation fluctuations, and the neutralized power output is smoothed and matches well with the forecasting wind generation. With time going from 04:00 to 07:00, an increasing number of responsive PEVs meets the non-responsive criterion and starts to charge with the rated power, and the capability of counterbalancing wind power fluctuation of PEVs deteriorates. Finally, the power compensation ability is completely lost during 07:00–08:00, and the neutralized power output considering PEV generation becomes exactly the same as the fluctuating wind power.

The frequency regulation performance is also compared between two scenarios: 1) The frequency is only controlled by the coal and diesel generators without PEVs; 2) The frequency is controlled by coal and diesel generators as well as PEVs by us-

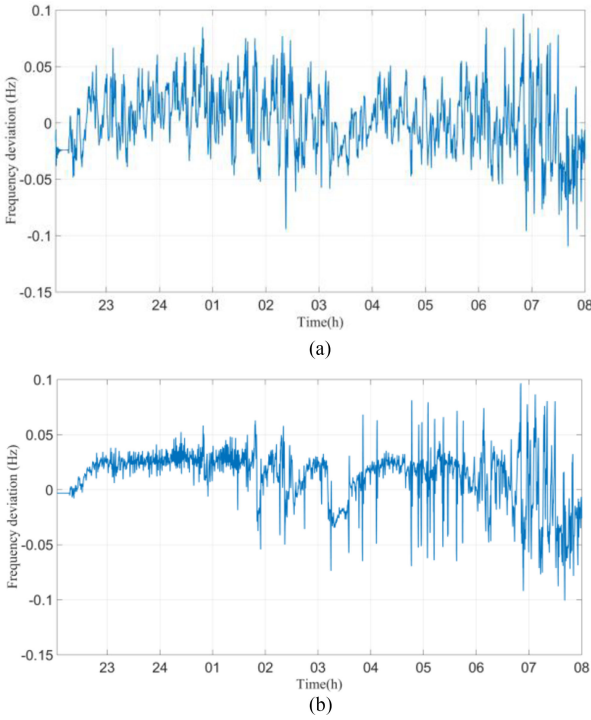


Fig. 11. Frequency deviation for the system with 16 PEVs and wind generations sampled every 8s. (a) Without PEVs (Mean = 0.0222 Hz, Max = 0.0978 Hz, Std = 0.0282 Hz). (b) With PEVs (Mean = 0.0217 Hz, Max = 0.0965 Hz, Std = 0.0260 Hz).

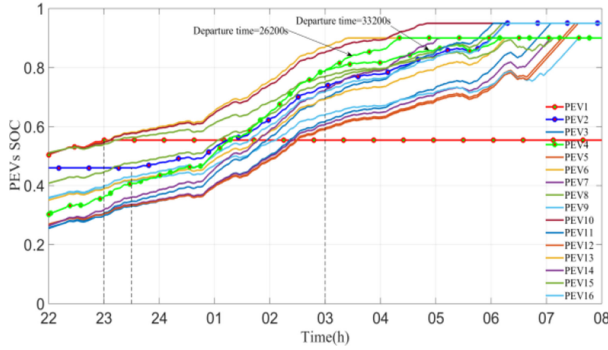


Fig. 12. SOC curves of 16 PEVs.

ing the proposed charging scheme. The frequency deviations of these two scenarios are shown in Fig. 11 with mean and standard deviation (Std) indicated in the bracket. The comparison results demonstrated that in a distribution system with fluctuating wind power generations, the proposed PEV charging scheme can effectively improve the frequency regulation performance when there are enough responsive PEVs due to PEVs' fast-response capability. However, with time going and the number of responsive PEVs reducing, the capability of PEVs for frequency regulation has certainly diminished.

The SOC curves of PEV₁ to PEV₁₆ with the charging behaviors discussed above is displayed in Fig. 12. When PEVs respond to neutralize the wind power fluctuation, all PEVs except PEV₁ (with earlier departure) finally achieve the satisfied SOC_{end} before the departure time T_i . To simulate the random

departure of PEV, PEV₁ is assumed to drop out the charging network at 23:00. With the proposed charging scheme, the SOC of PEV₁ is not changed during 23:00–08:00 as verified in Fig. 12. In addition, in practice PEV user might postpone to plug in PEV or randomly plug in PEV, and this circumstance is simulated by PEV₂. It can be found that the SOC of PEV₂ is constant until 23:30. After it is connected to the charging network, PEV₂ can correctly join in the proposed charging scheme and finish the SOC target as normal. Furthermore, the frequently changed departure time during charging process is also simulated by PEV₄. The user of PEV₄ changes the planned departure time from 26200s (around 05:15) to 33200s (around 07:10) at 03:00. In Fig. 12, PEV₄ accordingly slows down the charging power at 03:00, as it is not so urgent due to the extended departure time, and reaches the desired SOC_{end} a bit later. Therefore, it can be demonstrated that the proposed scheme could effectively handle the common practical driving patterns including the random arrival time, frequently changed departure time, the random initial and desired SOC, and correctly satisfy PEV charging requirements with the superior ancillary service of frequency regulation. The results have validated the plug-in and play capability of the proposed charging scheme.

To see how sample time could affect the effectiveness of the proposed scheme in term of frequency regulation, in the following section the PEV charging scheme is investigated for various sample time (e.g., 4s, 30s and 60s) of wind power fluctuations. As shown in Fig. 13, in general, the frequency deviations are all effectively regulated for these three scenarios at the beginning when with enough responsive PEVs. However, with time elapsing, the performances of the charging scheme in frequency regulation are similarly deteriorated for the three scenarios due to the reducing number of responsive PEVs. When further make specific comparisons of these results, as indicated by the frequency deviations in Figs. 13(a)–(c) and 11(b), Fig. 13(a) is with the smallest mean and Std value while Fig. 13(c) is with the largest mean and Std value. There is a tendency that with an increasing sample time of wind power fluctuations, the frequency deviations regulated by the proposed PEV charging scheme enlarge slightly. This is because that PEVs are generally electronic-based devices with fast ramping up/down power and thus could well follow up the rapidly changing wind power fluctuations. However, with sample time of wind power fluctuations increased, the capabilities of fast ramping up/down of multiple PEVs are not fully exploited to compensate the rapidly changing wind power fluctuations, thus the frequency regulation performance in Fig. 13(c) with the largest sample time is not as good as that in other scenarios.

VI. VALIDATING SCALABILITY OF THE PROPOSED SCHEME FOR FREQUENCY REGULATION

For case study 1 and 2, these 2000 PEVs are divided into 16 groups, and each group including 125 PEVs is assumed to connect to one aggregator. Afterwards the proposed fully distributed approach is implemented at each aggregator. However, there is no limitation for the proposed approach to handle even more distributed PEVs. In the following section, the original

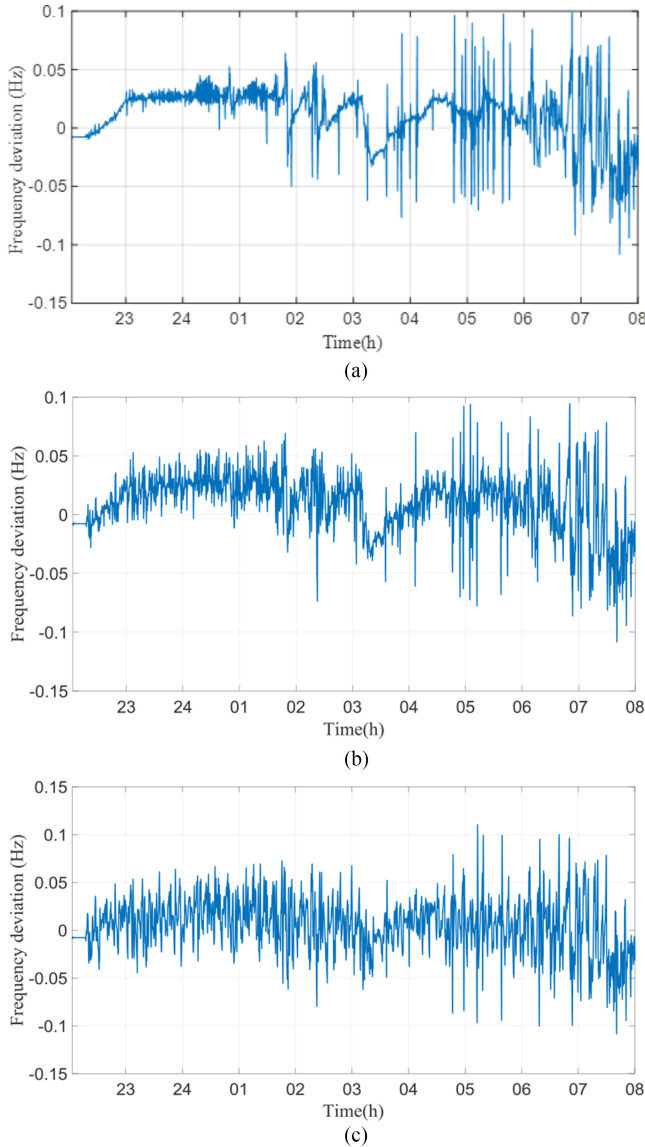


Fig. 13. Frequency deviation comparasions for the system with 16 PEVs and wind generations sampled at various periodic time. (a) for wind generation sampled every 4s (Frequency Std = 0.0246 Hz). (b) for wind generation sampled every 30s (Frequency Std = 0.0264 Hz). (c) for wind generation sampled every 120s (Frequency Std = 0.0268 Hz).

2000 PEVs will be expanded to divide into 50 groups (regarded as study case 3) for investigating the scalability of the proposed scheme for frequency regulation. It is expected that with good scalability, the proposed charging scheme shall be readily applied for more distributed PEVs such as for 2000 individual PEVs or several thousands of PEVs.

In this case, a communication topology for the 50 groups of PEVs is selected based on the aforementioned $n-1$ rule. In specific, each PEV_{*i*} ($i = 1, 2, \dots, 50$) is assumed to communicate with its adjacent neighbors with the index number $i + 1$ and $i + 10$ as shown in Fig. 14. The communication graph is connected with 100 links, while the maximum possible number of links for 50 PEVs is $C_{50}^2 = 1225$, so the density of the graph connectivity is only $100/1225 = 0.08$. Correspondingly, the communication coefficients are set according to (25). The

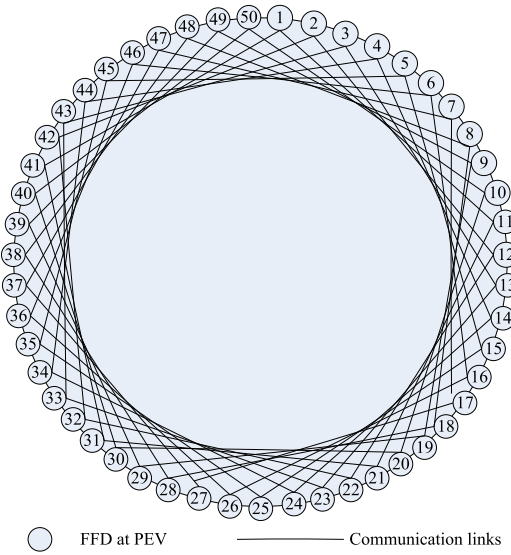


Fig. 14. Communication topology for 50 PEVs.

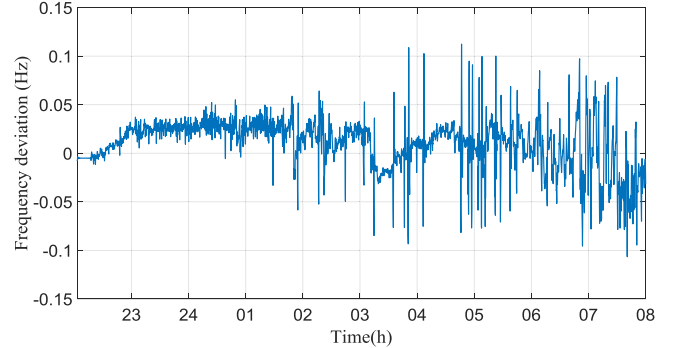


Fig. 15. Frequency deviation of the system with 50 PEVs and wind generations sampled every 8s. (Note: Frequency Max = 0.1123 Hz, Frequency Std = 0.0274 Hz).

parameters such as the initial SOC, the target SOC and the departure time of PEV₁ to PEV₅₀ are randomly generated, while the fluctuating wind power and the forecasting wind generation are the same as that in case 2 shown in Fig. 10, and the wind farm power fluctuations are sampled every 8s.

Fig. 15 plots the frequency deviations of the proposed algorithm applied to the distribution system with 50 groups of PEVs. It is evident that the proposed PEV charging scheme can also effectively regulate the system frequency. The maximal and Std value of the frequency deviation shown in Fig. 15 are 0.1123 Hz and 0.0274 Hz, which are comparable to the value for assessing the performance of the proposed algorithm with 16 groups of PEVs indicated in Fig. 11(b) of Section V-B.

Fig. 16 further plots the corresponding SOC curves of these 50 groups of PEVs, and the results show that each group PEV could approach a satisfactory SOC level before the randomly set departure time.

The comparisons between case study 2 in Section V-B and the case 3 demonstrates that with increasing number of distributed PEVs, the proposed PEV charging scheme could still effectively regulate the system frequency in the real time while the PEV

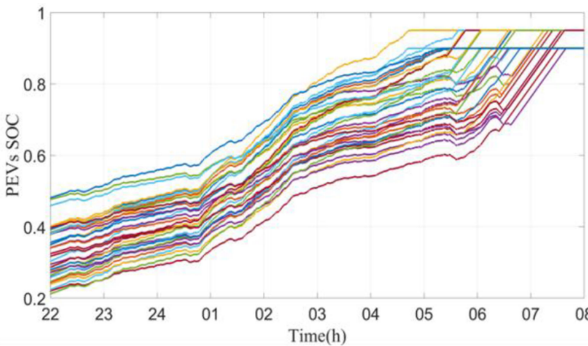


Fig. 16. SOC curves of the system with 50 PEVs.

users' charging requirements could be well satisfied. Therefore, the proposed charging scheme is with good scalability, and it is reasonable to expect that the scheme is capable of accommodating a large number of distributed PEVs for frequency regulation of a distribution power system, as its computational capability could be ensured by a reasonable communication network, for instance with the similar density of graph connectivity as shown in Fig. 14.

VII. CONCLUSION

In this paper, a comprehensive PEV charging model is presented to mitigate wind power fluctuations in a distribution system. While PEV users' daily driving requirements including the SOC target and departure time are modeled by the defined willing-to-pay parameter, PEV charging power is optimized to share the wind power fluctuations. On this basis, a fully distributed control scheme is designed to flexibly allocate the charging/discharging power of multiple PEVs in the real time. The scheme is robust to different PEVs driving patterns, such as their random plugging in and plugging out, initial SOC, desired SOC and the frequently changing departure time. Tests on the distribution system with wind farms, coal-diesel generators and multiple PEVs have demonstrated the effectiveness and robustness of the proposed control scheme in regulating system frequency as well as its good flexibility in satisfying PEVs charging demands with plug-in and play capability. Since the proposed PEV charging process to exclusively regulate system frequency would affect the power flows of the distribution networks and may result in operation constraint violations, such as violating the voltage limits and thermal limits, further ongoing research would elaborately design an PEV charging scheme (e.g., a bi-level on-line optimal power flow model) to simultaneously regulate system frequency and ensure operation static security of distribution systems.

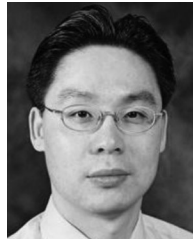
REFERENCE

- [1] G. Liu and K. Tomsovic, "Quantifying spinning reserve in systems with significant wind power penetration," *IEEE Trans. Power Syst.*, vol. 27, no. 4, pp. 2385–2393, Nov. 2012.
- [2] M. Q. Wang and H. B. Gooi, "Spinning reserve estimation in microgrids," *IEEE Trans. Power Syst.*, vol. 26, no. 3, pp. 1164–1174, Aug. 2011.
- [3] E. Nasrolahpour and H. Ghasemi, "A stochastic security constrained unit commitment model for reconfigurable networks with high wind power penetration," *Elect. Power Syst. Res.*, vol. 121, pp. 341–350, Apr. 2015.
- [4] S. Connolly, K. Parks and C. Janecek, "Wind Induced Coal Plant Cycling Costs and the Implications of Wind Curtailment for Public Service of Colorado," *Xcel Energy*, Denver, CO, USA, pp. 1–43, Aug. 2011.
- [5] Wikipedia, "Plug-in electric vehicle," 2017. [Online]. Available: https://en.wikipedia.org/wiki/Plug-in_electric_vehicle
- [6] D. Dallinger, S. Gerda, and M. Wietschel, "Integration of intermittent renewable power supply using grid-connected vehicles—A 2030 case study for California and Germany," *Appl. Energy*, vol. 104, pp. 666–682, Apr. 2013.
- [7] S. Bahrami and M. Parniani, "Game theoretic based charging strategy for plug-in hybrid electric vehicles," *IEEE Trans. Smart Grid*, vol. 5, no. 5, pp. 2368–2375, Sep. 2014.
- [8] M. E. Khodayar, L. Wu, and M. Shahidehpour, "Hourly coordination of electric vehicle operation and volatile wind power generation in SCUC," *IEEE Trans. Smart Grid*, vol. 3, no. 3, pp. 1271–1279, Sep. 2012.
- [9] H. Yang et al., "Operational planning of electric vehicles for balancing wind power and load fluctuations in a microgrid," *IEEE Trans. Sustain. Energy*, vol. 8, no. 2, Apr. 2017.
- [10] C. Sun, S. J. Moura, X. Hu, J. K. Hedrick, and F. Sun, "Dynamic traffic feedback data enabled energy management in plug-in hybrid electric vehicles," *IEEE Trans. Control Syst. Technol.*, vol. 23, no. 3, pp. 1075–1086, May 2015.
- [11] M. M. A. Abdelaziz, M. F. Shaaban, H. E. Farag, and E. F. El-Saadany, "A multistage centralized control scheme for islanded microgrids with PEVs," *IEEE Trans. Sustain. Energy*, vol. 5, no. 3, pp. 927–937, Jul. 2014.
- [12] M. H. Khooban et al., "A new load frequency control strategy for micro-grids with considering electrical vehicles," *Elect. Power Syst. Res.*, vol. 143, pp. 585–598, Feb. 2012.
- [13] S. Falahati, S. A. Taher, and M. Shahidehpour, "A new smart charging method for EVs for frequency control of smart grid," *Int. J. Elect. Power Energy Syst.*, vol. 83, pp. 458–469, Dec. 2016.
- [14] J. Meng et al., "Dynamic frequency response from electric vehicles considering travelling behavior in the Great Britain power system," *Appl. Energy*, vol. 162, pp. 966–979, Jan. 2016.
- [15] Y. Mu, J. Wu, J. Ekanayake N. Jenkins, and H. Jia, "Primary frequency response from electric vehicles in the great Britain power system," *IEEE Trans. Smart Grid*, vol. 4, no. 2, pp. 1142–1150, Jun. 2013.
- [16] T. Masuta and A. Yokoyama, "Supplementary load frequency control by use of a number of both electric vehicles and heat pump water heaters," *IEEE Trans. Smart Grid*, vol. 3, no. 3, pp. 1253–1262, Sep. 2012.
- [17] C. Ahn, C. Li, and H. Peng, "Optimal decentralized charging control algorithm for electrified vehicles connected to smart grid," *J. Power Sources*, vol. 196, no. 23, pp. 10369–10379, Dec. 2011.
- [18] H. Liu et al., "Decentralized vehicle-to-grid control for primary frequency regulation considering charging demands," *IEEE Trans. Power Syst.*, vol. 28, no. 3, pp. 3480–3489, Aug. 2013.
- [19] J. Tan and L. Wang, "A game-theoretic framework for vehicle-to-grid frequency regulation considering smart charging mechanism," *IEEE Trans. Smart Grid*, vol. 8, no. 5, pp. 2358–2369, Sep. 2017.
- [20] J. Tan and L. Wang, "Coordinated optimization of PHEVs for frequency regulation capacity bids using hierarchical game," in *Proc. 2015 IEEE Power Energy Soc. General Meeting*, Denver, CO, USA, 2015, pp. 1–5.
- [21] F. Zhong, "A distributed demand response algorithm and its application to phev charging in smart grids," *IEEE Trans. Smart Grid*, vol. 3, no. 3, pp. 1280–1290, Sep. 2012.
- [22] X. Luo, S. Xia, and K. W. Chan, "A decentralized charging control strategy for plug-in electric vehicles to mitigate wind farm intermittency and enhance frequency regulation," *J. Power Sources*, vol. 248, pp. 604–614, Feb. 2014.
- [23] F. Milano, "An open source power system analysis toolbox," *IEEE Trans. Power Syst.*, vol. 20, no. 3, pp. 1199–1206, Aug. 2005.
- [24] H. Huang and C. Y. Chung, "Coordinated damping control design for DFIG-based wind generation considering power output variation," *IEEE Trans. Power Syst.*, vol. 27, no. 4, pp. 1916–1925, Nov. 2012.
- [25] Y. Ota et al., "Autonomous distributed V2G (Vehicle-to-Grid) satisfying scheduled charging," *IEEE Trans. Smart Grid*, vol. 3, no. 1, pp. 559–564, Mar. 2012.
- [26] S. B. Peterson, J. Apt, and J. F. Whitacre, Lithium-ion battery cell degradation resulting from realistic vehicle and vehicle-to-grid utilization, *J. Power Sources*, vol. 195, no. 8, pp. 2385–2392, 2010.
- [27] Y. F. He, B. Venkatesh, and L. Guan, Optimal scheduling for charging and discharging of electric vehicles, *IEEE Trans. Smart Grid*, vol. 3, no. 3, pp. 1095–1105, Sep. 2012.
- [28] G. A., L. K., and S. R., "Congestion pricing and user adaptation," in *Proc. IEEE INFOCOM*, Jan. 2001, vol. 2, pp. 959–965.

- [29] Z. Zhang and M. Chow, "Convergence analysis of the incremental cost consensus algorithm under different communication network topologies in a smart grid," *IEEE Trans. Power Syst.*, vol. 27, no. 4, pp. 1761–1768, Nov. 2012.
- [30] A. Nedic, A. Ozdaglar, and P. A. Parrilo, "Constrained consensus and optimization in multi-agent networks," *IEEE Trans. Autom. Control*, vol. 55, no. 4, pp. 922–938, Apr. 2010.
- [31] M. Zhu and S. Martinez, "Discrete-time dynamic average consensus," *Automatica*, vol. 46, no. 2, pp. 322–329, Feb. 2010.
- [32] S. Sundhar Ram, A. Nedić, and V. V. Veeravalli, "Distributed stochastic subgradient projection algorithms for convex optimization," *J. Optim. Theory Appl.*, vol. 147, no. 3, pp. 516–545, Jul. 2010.
- [33] W. Su, H. Eichi, W. Zeng, and M. Y. Chow, "A survey on the electrification of transportation in a smart grid environment," *IEEE Trans. Ind. Informat.*, vol. 8, no. 1, pp. 1–10, Feb. 2012.
- [34] W. Su, W. Zeng, and M. Y. Chow, "A digital testbed for a PHEV/PEV enabled parking lot in a Smart Grid environment," in *Proc. 2012 IEEE PES Innov. Smart Grid Technol.*, Washington, DC, USA, 2012, pp. 1–7.
- [35] P. Kulshrestha, K. Swaminathan, M. Y. Chow, and S. Lukic, "Evaluation of ZigBee communication platform for controlling the charging of PHEVs at a municipal parking deck," in *Proc. 2009 IEEE Vehicle Power Propulsion Conf.*, Dearborn, MI, USA, 2009, pp. 1211–1214.



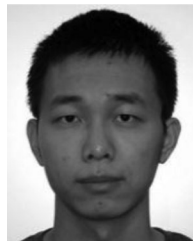
Xiao Luo received the B.Eng. (Hons.) and Ph.D. degrees in electrical engineering from Hong Kong Polytechnic University, Hong Kong, in 2011 and 2016, respectively. He is currently with the Department of Investment Planning, Huadian Power International Corporation, Ltd., Beijing, China. His major research interests include demand side management, renewable energy sources, microgrid, and power market.



Ka Wing Chan (M'98) received the B.Sc. (Hons.) and Ph.D. degrees in electronic and electrical engineering from the University of Bath, Bath, U.K., in 1988 and 1992, respectively. He is currently an Associate Professor and the Associate Head in the Department of Electrical Engineering, Hong Kong Polytechnic University, Hong Kong. His general research interests include power system stability, analysis and control, power grid integration, security, resilience and optimization, and demand response management.



Shiwei Xia (M'12) received the B.Eng. and M.Eng. degrees in electrical engineering from Harbin Institute of Technology, Harbin, China, in 2007 and 2009, respectively, and the Ph.D. degree in power systems from the Hong Kong Polytechnic University, Hong Kong, in 2015. He is currently with the State Key Laboratory of Alternate Electrical Power System with Renewable Energy Sources, School of Electrical and Electronic Engineering, North China Electric Power University, Beijing, China, and also with the Department of Electrical Engineering, Hong Kong Polytechnic University, Hong Kong. His research interests include security and risk analysis for power systems with renewable energies, distributed optimization, and control of multiple sustainable energy sources in smart grid.



Xi Lu received the B.Eng. degree in electrical engineering from North China Electric Power University, Beijing, China, in 2015. He is currently working toward the M.Phil. degree in electrical engineering at Hong Kong Polytechnic University, Hong Kong. His research interests include application of robust optimization and distributionally robust optimization in power system operation.



S. Q. Bu (S'11–M'12–SM'17) received the Ph.D. degree from the electric power and energy research cluster, The Queen's University of Belfast, Belfast, U.K., in 2012, where he continued his postdoctoral research work before entering industry. Subsequently, he joined National Grid UK as a Power System Engineer and then became an experienced UK National Transmission System Planner and Operator. He has received various prizes due to excellent performances and outstanding contributions in operational and commissioning projects. He is currently an Assistant Professor with The Hong Kong Polytechnic University, Kowloon, Hong Kong, and also a Chartered Engineer with UK Engineering Council, London, U.K.

His research interests are power system stability analysis and operation control, including wind power generation, PEV, HVDC, FACTS and ESS.